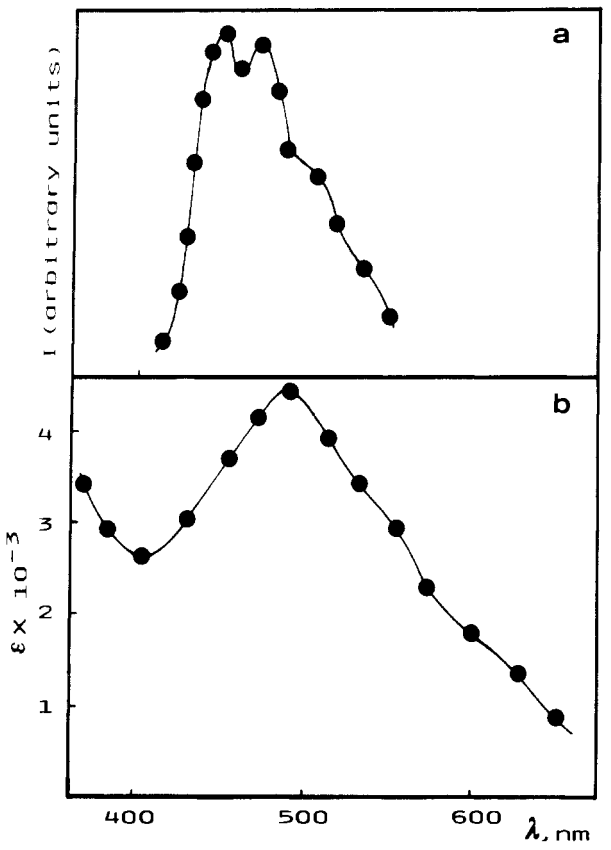

Figure 3. (a) Emission spectrum (see text) and (b) ESA spectrum of $Rh(phen)_2(CN)_2^+$ at room temperature in aqueous solution.

spectra can be analyzed as the superposition of a structured band with a 77 K like profile and a broad structureless band (Figure 4b). The relative importance of the structureless component increases with increasing temperature. The ratio between the areas (wavenumber scale) of the structureless and structured components gives an appreciably linear Arrhenius-type plot. Within the large error limits due to the narrow temperature range, the apparent activation energy and the preexponential factor are 0.11 ± 0.02 μm^{-1} and $\sim 10^3$, respectively. In the 150–200 K temperature range, the lifetimes of the structureless and structured component, while decreasing with increasing temperature, are always coincident. At room temperature, the complex is practically nonemitting.

The behavior of $Rh(phen)_2(NH_3)_2^{3+}$ in the 170–200 K temperature range clearly indicates the presence of *both* LC and MC emissions, with a MC/LC intensity ratio that increases with temperature. The identical lifetimes obtained for the two emissions probably indicate that the two states are in thermal equilibrium, i.e., $k_1 > (k_2 + k_3)$ and $k_{-1} > (k_4 + k_5)$.[18] In this hypothesis, the experimental "activation energy" (0.11 ± 0.02 μm^{-1}) of the MC/LC intensity ratio corresponds to the energy difference between the LC and MC states, and the preexponential factor ($\sim 10^3$) to the ratio of the radiative rate constants of the two states, k_4/k_2, neglecting entropy terms.[18] It is indeed known[13,19] that radiative rate constants for MC emissions are 2–3 orders of magnitude larger than those of LC phosphorescence of Rh(III) complexes. This explains why the MC emission can be observed even when, as in this case, the equilibrium fractional concentration

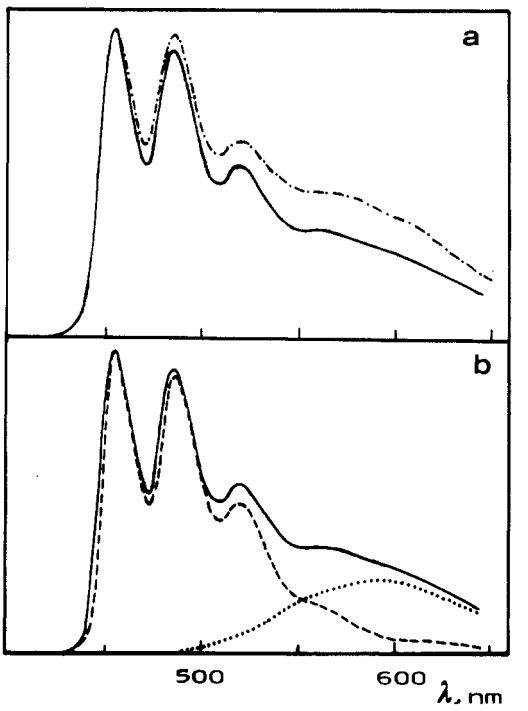

Figure 4. (a) Emission spectra of $Rh(phen)_2(NH_3)_2^{3+}$ at 177 K (—) and 186 K (·–·). (b) Analysis of the spectrum at 177 K as superposition of LC (– – –) and MC (···) component bands.

of this state is very small. It is expected that the fractional population of the MC state will further increase in going toward room temperature, although its observation is then hampered by the overall decrease in lifetime and intensity. The conclusion is that in $Rh(phen)_2(NH_3)_2^{3+}$ the MC excited state is sufficiently close in energy to the lowest LC state to be thermally accessible and give rise to observable dual emission. From this point of view, the behavior of $Rh(phen)_2(NH_3)_2^{3+}$ resembles that of $Rh(phen)_3^{3+}$, for which thermal population of the MC state and dual emission were previously observed.[6-8]

This work shows that, in complexes containing the $Rh(phen)_2^{3+}$ chromophoric unit, it is possible to tune the MC–LC energy gap by a suitable choice of the ancillary ligands so as to go from MC emitters ($Rh(phen)_2Cl_2^+$ and $Rh(phen)_2(NH_3)Cl^{2+}$) to LC emitters ($Rh(phen)_2(CN)_2^+$) through complexes that, in an appropriate temperature range, exhibit dual LC and MC emission ($Rh(phen)_2(NH_3)_2^{3+}$ and $Rh(phen)_3^{3+}$).

Acknowledgment. We thank L. Righetti for the drawings. This work has been supported by the Ministero della Università e della Ricerca Scientifica e Tecnologica and by the Consiglio Nazionale delle Ricerche (Progetto Finalizzato Chimica Fine).

(18) There is another limiting case in which the kinetic scheme of Figure 1b predicts identical lifetimes for the two emissions even in the absence of equilibrium ($(k_4 + k_5) > k_{-1}$): that in which the decay of MC is much faster than the MC → LC conversion ($(k_4 + k_5) > k_1$). In this case, the experimental "activation energy" of the intensity ratio would correspond to the difference between the activation energies of the k_1 and k_5 processes, and the preexponential factor would be equal to $(k_4/k_2)R$ where R is the ratio of the preexponential factors of k_1 and k_5.

(19) Crosby, G. A.; Watts, R. J.; Carstens, D. H. W. *Science (Washington, D.C.)* **1970**, *170*, 1195.

Contribution from the Departments of Chemistry, Portland State University, Portland, Oregon 97207-0751, and Washington State University, Pullman, Washington 99164-4630

Crystal Structure of $SF_5\overline{CHCF_2OSO_2}$

M. R. Pressprich, R. D. Willett,* R. J. Terjeson, R. Winter, and G. L. Gard*

Received November 6, 1989

Introduction

The preparation, reactions, and structure of β-fluorosultones are of considerable interest to chemists. Previously, we reported

* To whom correspondence should be addressed: R.D.W., Washington State University; G.L.G., Portland State University.

0020-1669/90/1329-3058$02.50/0

Table I. Crystallographic Data for $SF_5\overline{CHCF_2OSO_2}$

$C_2HO_3F_7S_2$	fw = 270.14
a = 10.881 (12) Å	space group: $P2_1/c$ (No. 14)
b = 5.149 (8) Å	T = −99 °C
c = 13.842 (15) Å	λ = 1.541 78 Å
α = 90°	ρ_{calcd} = 2.43 g cm^{-3}
β = 108.03 (8)°	μ = 78.2 cm^{-1}
γ = 90°	$R(F_o)$ = 0.069 (=0.070, all reflcns)
V = 737.4 (14) Å^3	$R_w(F_o)$ = 0.095 (=0.096, all reflcns)
Z = 4	

Table II. Non-Hydrogen Atomic Coordinates (×10^4) and Isotropic Thermal Parametes (Å^2 × 10^3) for $SF_5\overline{CHCF_2OSO_2}$

	x	y	z	U^a
S(1)	8357 (1)	2027 (3)	819 (1)	37 (1)
S(2)	5699 (1)	2558 (3)	1328 (1)	37 (1)
F(1)	9446 (3)	764 (7)	1694 (3)	50 (1)
F(2)	8260 (3)	−501 (7)	167 (2)	49 (1)
F(3)	8505 (3)	4605 (7)	1447 (2)	49 (1)
F(4)	7268 (3)	3321 (7)	−70 (2)	43 (1)
F(5)	9403 (4)	3056 (8)	355 (3)	56 (1)
F(6)	7553 (4)	−1567 (8)	2940 (3)	61 (2)
F(7)	8314 (4)	2265 (8)	3094 (3)	58 (2)
O(1)	5789 (4)	5268 (10)	1233 (3)	53 (2)
O(2)	4548 (4)	1250 (9)	827 (3)	48 (2)
O(3)	6166 (4)	1704 (10)	2513 (3)	52 (2)
C(1)	7401 (5)	734 (13)	2528 (4)	44 (2)
C(2)	7140 (5)	789 (11)	1393 (4)	32 (2)

[a] Equivalent isotropic U defined as one-third of the trace of the orthogonalized U_{ij} tensor.

Table III. Selected Non-Hydrogen Bond Lengths (Å) and Angles (deg) for $SF_5\overline{CHCF_2OSO_2}$

S(1)–F(1)	1.551 (4)	S(2)–O(2)	1.401 (4)
S(1)–F(2)	1.568 (4)	S(2)–O(3)	1.621 (5)
S(1)–F(3)	1.567 (4)	S(2)–C(2)	1.792 (6)
S(1)–F(4)	1.568 (4)	F(6)–C(1)	1.303 (8)
S(1)–F(5)	1.563 (5)	F(7)–C(1)	1.319 (7)
S(1)–C(2)	1.854 (7)	O(3)–C(1)	1.428 (8)
S(2)–O(1)	1.408 (5)	C(1)–C(2)	1.508 (8)
O(1)–S(2)–O(2)	120.5 (2)	F(6)–C(1)–O(3)	108.4 (5)
O(1)–S(2)–O(3)	110.8 (3)	F(7)–C(1)–O(3)	109.4 (5)
O(2)–S(2)–O(3)	108.8 (3)	S(2)–C(1)–C(2)	51.9 (3)
O(1)–S(2)–C(2)	115.0 (3)	F(6)–C(1)–C(2)	115.5 (5)
O(2)–S(2)–C(2)	114.5 (3)	F(7)–C(1)–C(2)	118.2 (6)
O(3)–S(2)–C(2)	79.4 (3)	O(3)–C(1)–C(2)	96.0 (4)
C(1)–S(2)–C(2)	41.5 (3)	S(1)–C(2)–S(2)	122.2 (3)
S(2)–O(3)–C(1)	96.3 (4)	S(1)–C(2)–C(1)	121.6 (4)
F(6)–C(1)–F(7)	108.2 (4)	S(2)–C(2)–C(1)	86.7 (4)

the preparation and reaction chemistry of $SF_5\overline{CHCF_2OSO_2}$.[1] In general, β-fluorosultones are covalent liquids at room temperature,[2,3] and it was surprising to find that $SF_5\overline{CHCF_2OSO_2}$ existed as a solid. While the ^{19}F and ^{13}C spectral data of $SF_5\overline{CHCF_2OSO_2}$ favored a cyclic structure, a crystal structure was carried out in order to obtain cyclic and exocyclic parameters and to understand the solid-state nature of this material. We wish to report, for the first time, the crystal structure of a β-fluorosultone.

Results and Discussion

X-ray structure analysis confirms the cyclic nature of the $SF_5\overline{CHCF_2OSO_2}$ sultone. Selected non-hydrogen bond lengths and angles are presented in Table III. As seen in Figure 1, the compound contains a four-membered sultone ring consisting of two carbon atoms, one sulfur atom, and one oxygen atom. The

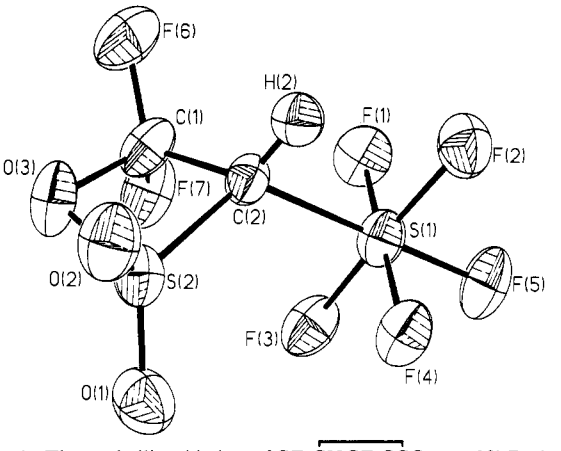

Figure 1. Thermal ellipsoid view of $SF_5\overline{CHCF_2OSO_2}$ at 50% Probability.

Table IV. Four-Membered 1,2-Oxathietanes

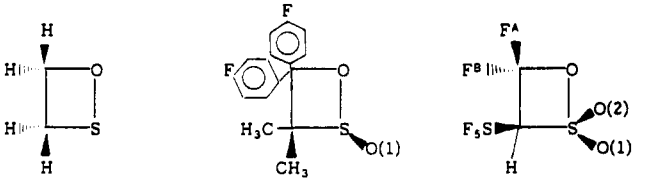

1 2 3

	1	2	3
	Ring Bond Lengths (Å)		
SO	1.669	1.667 (4)	1.621 (5)
SC	1.81[a]	1.856 (4)	1.792 (6)
CO	1.43[a]	1.487 (5)	1.438 (8)
C–C	1.581[a]	1.588 (1)	1.508 (8)
	Nonring Bond Lengths (Å)		
C–H =	1.105[a]		0.960[a]
SO(1)=		1.466 (4)	1.408 (5)
SO(2)=			1.401 (4)
	Ring Bond Angles (deg)		
SCC	89.3	86.4	86.7 (4)
OCC	92.7	93.8	96.0 (4)
CSO	100.6	79.0	79.4 (3)
dihedral		20.3	14.0
			13.7

[a] Assumed values.

ring is very distorted, with respect to both distances and planarity. The S(2)–O(3), O(3)–C(1), C(1)–C(2), and C(2)–S(2) distances are 1.621 (5), 1.428 (8), 1.508 (8), and 1.792 (6) Å, respectively, while the fold angles across O(3)–C(2) and S(2)–C(1) are 14.0 and 13.7°, respectively. The terminal S–O bond distances are approximately 0.2 Å shorter than that in the sultone ring. In contrast, the C–S bond distance to the SF_5 group is longer by 0.06 Å than the C–S distance in the ring. As discussed below, the packing appears to be dictated by relatively strong C–H···O hydrogen-bonding interactions between molecules. This would appear to be the reason for the observation of a crystalline phase at room temperature, in contrast to most other sultones.

In Table IV, a comparison of bond angles and lengths is given for the three four-membered ring systems: 1,2-oxathietane (**1**), a 1,2-oxathietane 2-oxide (β-sultine) (**2**), and a 1,2-oxathietane 2,2-dioxide (β-sultone) (**3**).[4,5] For the hypothetical compound **1** many of the reported values are assumed and, in light of trends found for compounds **2** and **3**, should be reexamined.[4] For example, the cyclic bond distances for S–O and S–C increase from compound **1** to **2** but decrease from compound **2** to **3**. It is

(1) Terjeson, R. J.; Mohtasham, J.; Gard, G. L. *Inorg. Chem.* **1988**, *27*, 2916.
(2) England, D. C.; Dietrich, M. A.; Lindsey, R. V. *J. Am. Chem. Soc.* **1960**, *82*, 6181.
(3) Canich, J. M.; Ludvig, M. M.; Gard, G. L.; Shreeve, J. M. *Inorg. Chem.* **1984**, *23*, 4403.
(4) Snyder, J. P.; Carlsen, L. *J. Am. Chem. Soc.* **1977**, *99*, 2931.
(5) Gray, M. D. M.; Russell, D. R.; Smith, D. J. H.; Durst, T.; Gimbarzevshy, B. *J. Chem. Soc., Perkin Trans. 1* **1981**, 1826.

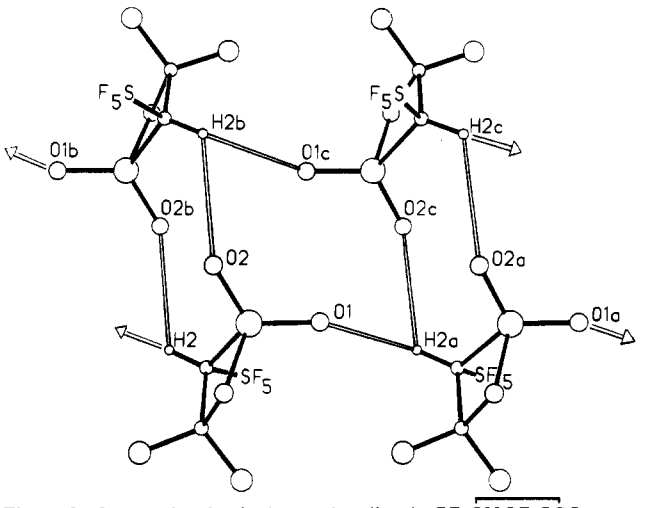

Figure 2. Intermolecular hydrogen bonding in $SF_5CHCF_2OSO_2$.

expected that these bond distances should decrease in going from the oxathietane (**1**) to the β-sultine (**2**) to the β-sultone (**3**) because of the increasing oxidation state of sulfur; this effect is seen in the shorter nonring SO bond distance for **3** versus **2**. A comparison of the bond angles for **1**–**3** shows good agreement for compounds **2** and **3**; for compound **1**, the bond angles were determined by assuming a planar four-membered ring. While compound **1** was assumed to be planar, compounds **2** and **3** are puckered with dihedral angles of 20.3[5] and (14.0, 13.7°), respectively. It is interesting to note that for perfluorocyclobutane a dihedral angle of 17.4° is found.[6] The values of the angles about sulfur, F-S(1)-F and C(2)-S(1)-F, correspond to a nearly octahedral arrangement of atoms bonded to S(1), with a maximum deviation of 2.9 (2)° in the F(2)-S(1)-F(3) angle (∠F-S-F = 177.1 (2)°).

Figure 2 shows a schematic ball and stick drawing of the intermolecular hydrogen bonding network of $SF_5CHCF_2OSO_2$. The C-H···O interactions are represented by open lines; those with arrowheads show interactions to neighboring, unpictured molecules. Lower case letters are used to distinguish symmetry-equivalent atoms. The hydrogen atom on one molecule forms a bifurcated interaction to a terminal oxygen atom on two other molecules. All hydrogen atoms and terminal oxygen atoms are therefore involved in intermolecular interactions. Several C-H···O interactions are shown in the figure, but only two are symmetry inequivalent: C(1)-H(2)···O(1)′ = 3.177 Å (∠C-H···O = 120.6°) and C(1)-H(2)···O(2)′ = 3.230 Å (∠C-H···O = 120.8°), where primes indicate atoms on neighboring molecules. These distances are long compared to normal interactions involving O-H and N-H groups (2.3 – 2.8 Å) but are comparable to the value of 3.2 Å reported for $(HCN)_n$.[7] There is little doubt that the hydrogen-bond network is responsible for the solid-state nature of $SF_5CHCF_2OSO_2$ at room temperature.

Experimental Section

The sultone $SF_5CHCF_2OSO_2$ was prepared according to the literature;[1] storage of the solid at room temperature under nitrogen at 1 atm resulted in formation of crystals acceptable for X-ray analysis. Examination of representative crystals under a polarizing microscope showed them to be optically biaxial but not sharply extinguishing.

Obtaining an acceptable X-ray data set was difficult due to the crystal quality problem mentioned above and also due to decomposition problems. When exposed to moisture, the crystals readily hydrolyze, and when exposed to pressures of less than an atmosphere at room temperature, they quickly sublime away. Sealed capillary methods were unsuccessful. More skillful drybox methods may have resolved the difficulties but were found to be unnecessary. Instead, an acceptable data set was obtained by using lower temperature techniques. A large crystal was cut by razor blade to a slightly larger than optimum size (≈0.8 mm cube). The crystal was attached by epoxy to a thin glass fiber and immersed in a -99 °C N_2 stream on a Nicolet R3m/E diffractometer system equipped with graphite-monochromated Cu Kα radiation. These steps were carried out under standard conditions but with haste (≈15 s). The resulting mounted crystal, nearly spherical in shape, 0.5 mm × 0.6 mm × 0.6 mm, was stable at the lowered temperature and showed no significant degradation during data collection. Peak scans showed the mounted crystal to be single-domain but to have very broad peak profiles. Subsequent Wycoff-ω data collection required peak scans of 2°.[8]

A total of 664 unique observed reflections, $|F_o| > 3\sigma(F_o)$ $\leq 2\theta \leq 100°$, were reduced to structure factor magnitudes by correction for Lorentz and polarization effects. Structure solution programs[9] led to resolution of all atomic positions. The hydrogen atom position was nevertheless constrained to C-H = 0.96 Å. All non-hydrogen atoms were refined anisotropically. The isotropic hydrogen atom thermal parameter was constrained to 1.2 times the equivalent isotropic parameter of the corresponding carbon atom. Crystal data are presented in Table I.

Acknowledgment. We wish to express our appreciation to the U.S. Department of Energy, Grant No. DE-FG21-88MC25142, for support of this work. The X-ray diffraction facility was established through funds from the NSF (Grant No. CHE-8404807) and the Boeing Co.

Supplementary Material Available: Full listings of data collection and refinement parameters, anisotropic thermal parameters, and hydrogen atom positions a unit cell packing diagram and (4 pages); a table of observed and calculated structure factors (4 pages). Ordering information is given on any current masthead page.

(6) Chang, C. H.; Porter, R. F.; Bauer, S. H. *J. Mol. Struct.* **1971**, *7*, 89.
(7) Dulmage, W. J.; Lipscomb, W. N. *Acta Crystallogr.* **1951**, *4*, 330.
(8) Campana, C. F.; Sheperd, D. F.; Litchman, W. N. *Inorg. Chem.* **1980**, *20*, 4039.
(9) Sheldrick, G. M. *SHELXTL Users Manual*, version 5.1; Nicolet Instrument Corp.: Madison, WI, 1986.

Contribution from the Departments of Chemistry, University of Minnesota, Minneapolis, Minnesota 55455, and Cornell University, Ithaca, New York 14853

Proton Nuclear Magnetic Resonance Studies of Iron(II/III)-Amide Complexes. Spectroscopic Models for Non-Heme Iron Proteins

Li-June Ming,† Randall B. Lauffer,‡ and Lawrence Que, Jr.*,†

Received October 25, 1989

Proton NMR spectroscopy has been a useful tool for investigating the metal binding site(s) of metalloproteins via the detection of the isotropically shifted proton signals.[1] While iron has successfully served as an intrinsic probe for the study of the active-site configuration of heme proteins and iron–sulfur proteins using several different NMR techniques,[1,2] its use as an NMR probe in other non-heme proteins is still not widely adopted and needs further exploration. The successful observation of isotropically shifted ^1H NMR signals of the iron-coordinated amino acid residues in the non-heme iron protein uteroferrin[3] has triggered studies on non-heme iron proteins by the use of NMR spectroscopy.[4] Features observed in the ^1H NMR spectrum of uteroferrin have been assigned to the histidyl imidazole protons and the tyrosyl protons.[3,5] Interestingly, an upfield-shifted solvent-exchangeable signal was also observed in the ^1H NMR spectrum that could not be assigned to an imidazole NH proton of a coordinated histidine residue[3,5] but could possibly arise from an NH proton of a peptidyl moiety coordinated through the carbonyl oxygen.[3,5] Alternatively, this signal may arise from a solvent-exchangeable proton in the proximity of the metal center upfield shifted via a dipolar shift mechanism.[1] In this paper, a

† University of Minnesota.
‡ Cornell University. Present address: NMR Section, Department of Radiology, Massachusetts General Hospital and Harvard Medical School, Boston, MA 02114.

0020-1669/90/1329-3060$02.50/0